Apoptosis (2007) 12:1569–1577
DOI 10.1007/s10495-007-0089-1

ORIGINAL PAPER

Mitochondrion-mediated apoptosis induced by *Rana grylio* virus infection in fish cells

You-Hua Huang · Xiao-Hong Huang · Jian-Fang Gui · Qi-Ya Zhang

Published online: 6 June 2007

Abstract A fish cell line, fathead minnow (FHM) cell, was used to investigate the alteration of mitochondrial dynamics and the mechanism of apoptosis under *Rana grylio* virus (RGV) infection. Microscopy observations, flow-cytometry analysis and molecular marker detection revealed the apoptotic fate of the RGV-infected cells. Some typical apoptotic characteristics, such as chromatin condensation, DNA fragmentation and mitochondrial fragmentation, were observed, and significantly morphological changes of mitochondria, including size, shape, internal structure and distribution, were revealed. The mitochondria in RGV-infected cells were aggregated around the viromatrix, and the aggregation could be blocked by colchicine. Moreover, the $\Delta\psi$m collapse was induced, and caspase-9 and caspase-3 were activated in the RGV-infected cells. In addition, NF-κB activation and intracellular Ca^{2+} increase were also detected at different times after infection. The data revealed the detailed dynamics of mitochondrion-mediated apoptosis induced by an iridovirus, and provided the first report on mitochondrial fragmentation during virus-induced apoptosis in fish cells.

Keywords Fish cell · Apoptosis · Mitochondrion · Mitochondrial fragmentation · *Rana glylio* virus (RGV) · Caspase

Y.-H. Huang · X.-H. Huang · J.-F. Gui · Q.-Y. Zhang (✉)
State Key Laboratory of Freshwater Ecology and Biotechnology, Institute of Hydrobiology, Chinese Academy of Sciences, Graduate School of the Chinese Academy of Sciences, Wuhan 430072, China
e-mail: Zhangqy@ihb.ac.cn

Introduction

Apoptosis is a highly regulated cell death process that usually results in the cell demise. It is often activated during normal development and in response to diverse stimuli [1]. Mitochondria, which are well-known multifunctional organelles, play prominent roles in supplying energy and regulating apoptosis [2–4]. Recently, mitochondrial dynamics and the dramatic alterations, such as mitochondrial fragmentation and crista remodeling, have been reported during the early stages of apoptosis [5–7].

Virus infection has been observed to be associated with apoptosis [8–11], and the molecular mechanisms and signal pathways have been disclosed in virus infection of mammal cells [12, 13]. Apoptosis of fish cells can be also triggered by virus infection [14–16], but systematic studies on mitochondrial dynamics and the molecular mechanisms are very limited. In our previous studies, an iridovirus isolated from the cultured pig frog (*Rana grylio*), which is called *Rana grylio* virus (RGV), has been characterized [17], and a similar apoptotic process has been observed in RGV infected fish cells [18]. Electron microscopic observation displayed large clusters of mitochondria around the viromatrix in the infected cells [18]. The preliminary results imply that RGV infection induces apoptosis, and that the apoptotic process and mechanism might be mitochondrion-mediated. In this study, we further observe and analyze the mitochondrial dynamics during RGV infection, and investigate the regulative mechanism in the infected fathead minnow (FHM) cells. The current results provide the first report on mitochondrial fragmentation during virus infection in fish cells, and reveal mitochondrion-mediated pathway in the RGV infection-induced apoptosis.

Methods

Cell and virus

RGV is an important pathogenic iridovirus isolated from cultured pig frog [19]. Fathead minnow (FHM) cell, a fish cell line, was used in this study. Cells were grown in TC199 with 10% fetal calf serum (FCS, GIBCO) and were infected with RGV at a multiplicity of infection (MOI) of 1.

Cell transfection

To observe subcellular distribution of mitochondria in RGV-infected cells, pDsRed2-Mito (BD Bioscience Clontech), expressing a fusion protein of *Discosoma* sp. red fluorescent protein linked to the mitochondrial targeting sequence, was used. Prior to transfection, FHM cells were grown to 80% confluence and transfected using the Lipofectamine 2000 (Invitrogen) transfection reagent according to the manufacturer's instructions. Cells were selected in medium containing G418 (400 μg/ml) for 3 weeks followed by maintaining in medium with G418 (200 μg/ml). Stable clones were subsequently expanded for further analysis.

Transmission electron microscopy

Mock- and RGV-infected cells were harvested by scraping the cells into the medium, respectively, followed by centrifugation at 700*g* for 10 min. Sample preparation was performed as previously described [18]. The grids containing ultrathin sections were examined with a JEM-1230 electron microscopy at 100 KV and micrographs were taken by CCD camera.

Hoechst staining and fluorescence microscopy

To visualize nuclear morphology and show the viromatrix, Hoechst 33258 (Sigma) was used as a marker. Mock- and RGV-infected FHM cells were fixed with 4% paraformaldehyde and then stained with 1 μg/ml of Hoechst 33258 in PBS buffer for 20 min. After three washes in PBS buffer, cells were visualized by fluorescence microscopy (Leica, DMIRB) using an ultraviolet (UV) excitation filter and images were processed using the Adobe Photoshop program.

To clarify possible approach of mitochondrial transport in RGV-infected cells, colchicine was used to disassemble microtubules. Cells stably expressing pDSRED2-mito were cultured in 6-well plates and infected with RGV for 8 h, 18 h. Another set was carried out: 0.5 μM colchicine (Sigma) was added to mock- and RGV-infected cultures at 6 h postinfection (p.i.). Then cells were stained with Hoechst 33258 and observed as described above.

Measurement of cellular DNA content

Mock- and RGV-infected cells were harvested, washed with PBS and fixed in 70% ice-cold ethanol overnight at –20°C. The collected cells were washed with PBS again and fixed with 70% ethanol overnight at –20°C. After washing with PBS again, the cells were stained with PBS containing 50 μg/ml of propidium iodide (Sigma) and 100 μg/ml of DNase-free RNase A for 30 min. Flow-cytometric measurement of 1×10^4 cells was carried out in a fluorescence activated cell sorter (Beckman-Coulter Epics Altra) and analyzed using the CellQuest program.

DNA fragmentation assay

Mock- and RGV-infected cells were harvested, and the total genomic DNA was extracted according to methods described previously [20]. Briefly, the collected cells were lysed with TES (10 mM Tris, pH 8.0, 1 mM EDTA, 1% SDS, 100 μg/ml of proteinase K), and the lysate was incubated at 50°C for 3 h. DNA was precipitated with 70% (v/v) ethanol at –20°C overnight and then by centrifugation at 12,000*g* for 15 min. The DNA pellet was washed with 70% ethanol, dried and resuspended in distilled water with RNase A (50 μg/ml), then analyzed by 2% agarose gel electrophoresis.

Determination of mitochondrial membrane potential ($\Delta\psi$m)

Rhodamine 123 (Rh123) is an aromatic cation, it distributes electrophoretically into the mitochondrial matrix across the inner membrane in response to $\Delta\psi$m. Changes in $\Delta\psi$m were evaluated with Rh123, which is taken up by intact mitochondria and released upon permeability transition of the mitochondria [21]. Mock- and RGV-infected cells were isolated by centrifugation (200*g*, 10 min) and resuspended in 0.6 ml PBS containing 10 μg/ml of Rh123 (Sigma). Cells were incubated for 30 min at 25°C, and then centrifuged. After washing with PBS, the cells were resuspended in 1 ml PBS and analyzed on a flow cytometry (Beckman-Coulter Epics Altra). In each plot, the region of E shows the percentage of cells with decreased $\Delta\psi$m, and the region of C shows the percentage of cells with normal $\Delta\psi$m.

Analysis of caspase activity

To investigate the caspase-3 and caspase-9 activity during RGV infection, Ac-DEVD-AMC (substrate for caspase-3) and Ac-LEHD-AFC (substrate for caspase-9) (Calbiochem) were used. Mock- and RGV-infected cells were collected from monolayers, and then lysed in 100 μl of

lysis buffer (20 mM HEPES-KOH, pH 7.5, 250 mM sucrose, 50 mM KCl, 2.5 mM $MgCl_2$, 1 mM dithiothreitol, 1‰ CHAPS, 20 mg/ml leupeptin, 10 mg/ml aprotinin) for 1 h at –70°C. After centrifugation, 10 µl of supernatant was added to 189 µl of caspase assay buffer (20 mM HEPES-KOH, pH 7.5, 250 mM sucrose, 50 mM KCl, 2.5 mM $MgCl_2$, 10 mM dithiothreitol, 1‰ CHAPS) with a final concentration of 20 µM Ac-DEVD-AMC or Ac-LEHD-AFC. The reaction mixtures were incubated at 37°C for 1 h. Levels of cleaved caspase substrate were measured using a spectrofluorometer (Molecular Devices) with an excitation wavelength of 380 nm and an emission wavelength of 460 nm. The data were expressed as fold increase compared to the corresponding values of caspase activity in lysates of mock-infected cells.

Assay for Ca^{2+} mobilization

The intracellular Ca^{2+} in individual FHM cells was measured using the cell permeant Ca^{2+} sensitive fluorescent dye Fluo-3 acetoxymethyl ester (Fluo-3 AM). After the medium was removed from the culture plates, cells were washed with Ca^{2+}-free PBS and incubated with 500 µl of 4 µM Fluo-3 acetoxymethyl ester diluted in HBSS buffer (10 mM D-glucose, 120 mM NaCl, 4.5 mM KCl, 0.7 Mm Na_2HPO_4, 1.5 mM NaH_2PO_4 and 0.5 mM $MgCl_2$ (pH 7.4)) for 20 min. Then, 2.5 ml of HBSS buffer containing 1% BCS were added into the samples and further incubated for 40 min. Following the trypsinization, cells were harvested and washed twice in 2 ml of Ca^{2+}-free PBS at 25°C. After pelleting by centrifugation, the cells were resuspended in 1 ml of Ca^{2+}-free PBS at 25°C, and analyzed immediately by flow cytometry. Approximate 10,000 cells were analyzed for each sample. The region of D in the plot shows the percentage of cells, which have an increased intracellular Ca^{2+} and higher Fluo-3 fluorescence intensity.

Reporter gene assays

The activation of NF-κB by RGV infection was measured by NF-κB dependent luciferase reporter construct (NF-κB-luc, Clontech), which contains four NF-κB binding sites upstream of the luciferase gene. Briefly, FHM cells (4×10^5) in 24-well tissue culture plates were transfected with 80 ng of NF-κB-luc and 20 ng of cytomegalovirus β-galactosidase reporter construct as described above. After incubation for 24 h, cells were either mock-infected or infected with RGV at an MOI of 10 and incubated at 25°C for various intervals. Then, cells were harvested and analyzed for luciferase expression using luciferase assay system (Promega) following manufacturer's instruction. Samples were also assayed for β-galactosidase activity using β-galactosidase enzyme assay system (Promega) to normalize for transfection efficiency.

Results

Morphological changes of RGV infection-induced apoptosis in FHM cells

Apoptotic morphological changes of the RGV-infected FHM cells were firstly examined by microscopy. As shown in Fig. 1A, some typical morphological changes, such as extreme chromatin condensation and nucleus fragmentation, are observed under electron microscopy in a RGV-infected FHM cell in which there exist abundant RGV

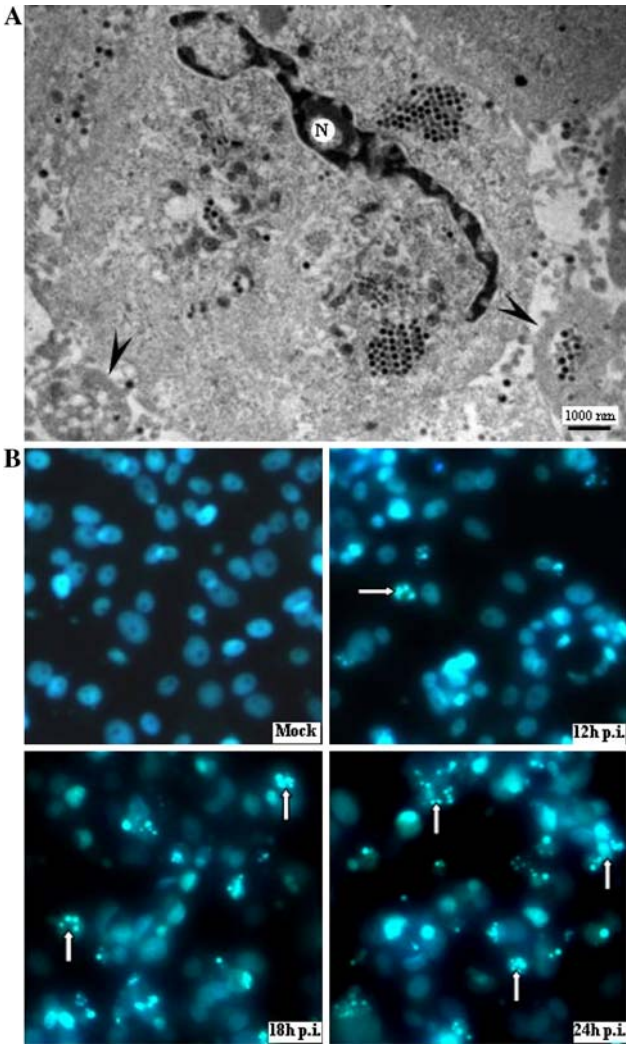

Fig. 1 Apoptotic morphological changes in the RGV-infected FHM cells. (**A**) Transmission electron microscopy observation. Black arrowheads indicate the apoptotic bodies. (**B**) Nuclear fragmentation in the RGV-infected FHM cells at different times after infection. Arrows indicate the fragmental nucleus

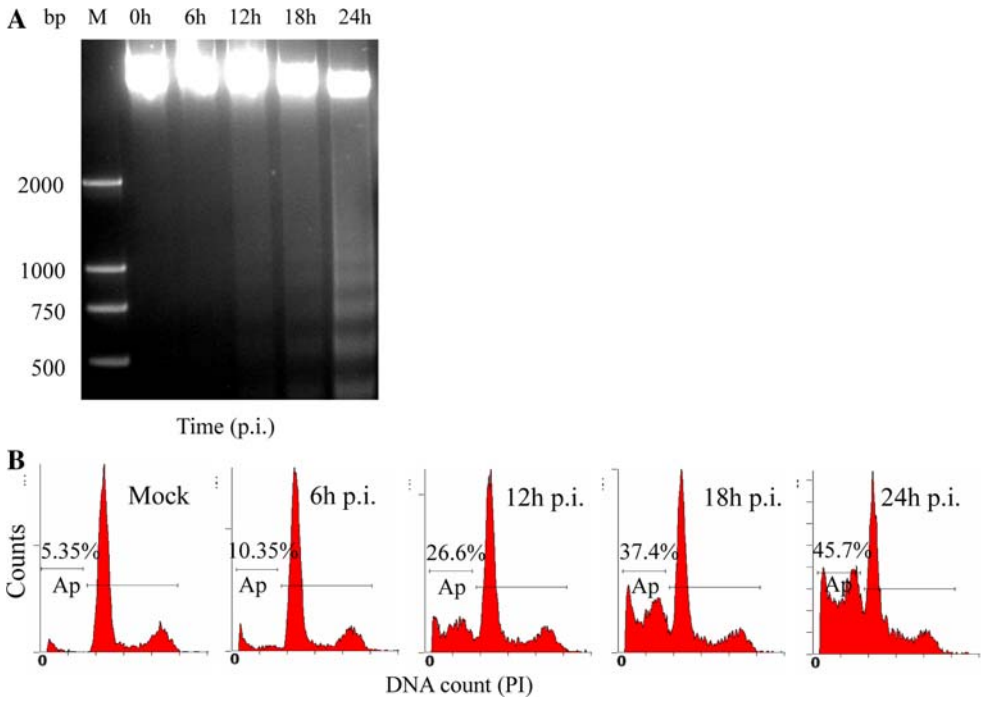

Fig. 2 Induction of DNA fragmentation and the DNA content analysis. (**A**) DNA fragmentation at different times after infection. (**B**) DNA contents quantified by flow cytometry. The population of cells that contain sub-G1 levels of DNA are indicated on the histogram by the bar marked Ap. The percentage of apoptotic cells was calculated by Sub-G1 population/total cell cycle populations

particles. Moreover, fluorescence microscopy observation showed apoptotic dynamics of the RGV-infected FHM cells under different infection times. As shown in Fig. 1B, obvious apoptotic changes are observed at 12 h p.i., and as the infection time increases, more and more cells undergo nuclear fragmentation and the formation of apoptotic bodies. In contrast, mock-infected cells possess uniformly stained nuclei (Fig. 1B).

DNA fragmentation was examined in the RGV-infected FHM cells. As shown in Fig. 2A, the DNA fragment ladder begins to appear at 12 h p.i. as the cytopathic effect (CPE) occurs in the RGV-infected FHM cells, and the DNA fragmentation intensity increases along with the CPE increases. In comparison with the RGV-infected cells, an intact chromosomal DNA band without laddering effect was observed in mock-infected cells (Fig. 2A).

To quantify the percentage of apoptotic cells, the RGV-infected and mock-infected cells were stained with propidium iodide (PI), and measured by flow cytometry. As shown in Fig. 2B, the proportion of apoptotic cells in RGV-infected cells increases from 10.35% at 6 h p.i. to 45.63% at 24 h p.i., whereas apoptosis appears only in 5.35% mock-infected cells.

Morphological changes of mitochondria during RGV infection

Ultrastructural observations revealed significantly morphological changes of mitochondria in the RGV-infected fish cells. As shown in Fig. 3, in contrast with oval and rod-shape mitochondria with normal cristae in cytoplasm of the mock-infected cells (Fig. 3A), the shape and size of mitochondria obviously display fragmentation characteristics, which result in small and numerous organelles. The cristae are distorted and the number of them badly decreases, only few cristae structures are observed in most of the fragmented mitochondria (Fig. 3B). Numerous dumbbell-shaped mitochondria with a narrow interconnecting isthmus are observed in the RGV-infected FHM cells, and most of them are distributed around the viromatrix (Fig. 3C).

Distribution changes of mitochondria in RGV-infected cells

Subcellular distribution changes of mitochondria were further confirmed by fluorescence microscopy in the stably tansfected pDsRed2-Mito FHM cells. As shown in Fig. 4, in contrast to even distribution throughout the cytoplasm in mock-infected FHM cells (Fig. 4A), some viromatrix occur in the nuclear proximity, and most of mitochondria appear to aggregate toward the viromatrix in the RGV-infected cells (Fig. 4B). As the infection time increases, the area and number of the viromatrix increase, and almost all of the mitochondria are gathered around the viromatrix at 18 h p.i. (Fig. 4C).

Preliminary experiments indicated that treatment of FHM cells with 0.5 μM colchicine could result in microtubule disassembly, and no obvious cell toxicity was observed (data not shown). Therefore, the concentration of colchicine was

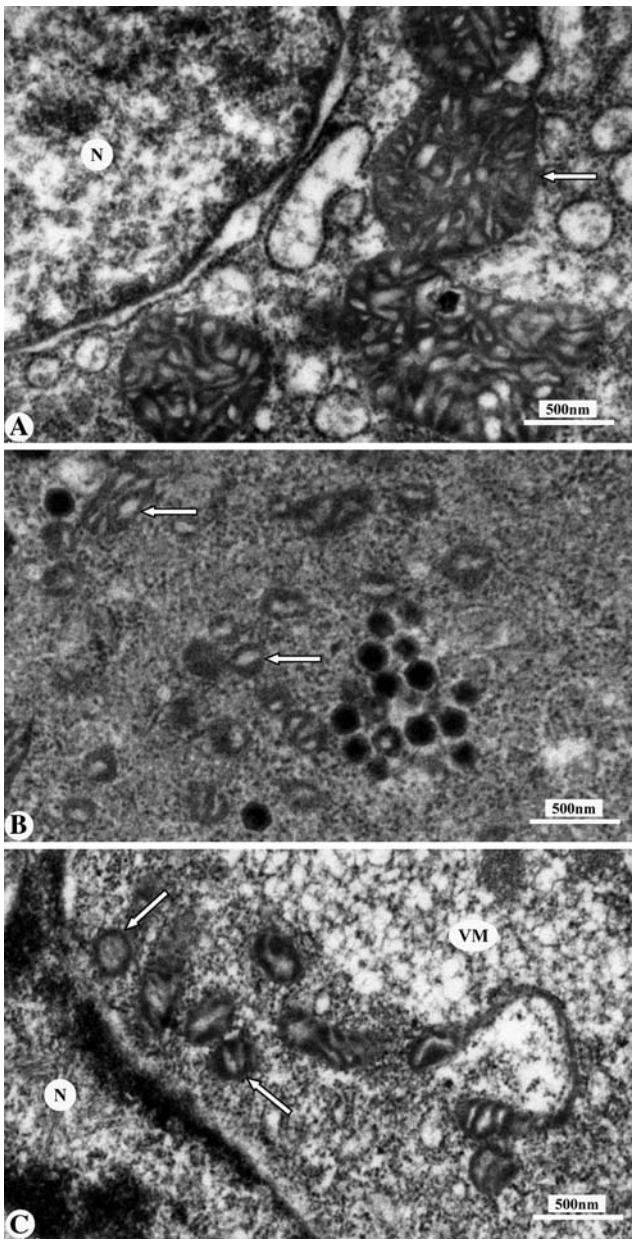

Fig. 3 Ultrastructural observations of mitochondria in the RGV-infected FHM cells. (**A**) Normal mitochondria in the control FHM cell. (**B**) and (**C**) The abnormal mitochondria in the RGV-infected FHM cells. VM: Viromatrix; N: Nucleus. Arrows indicate the mitochondria, and white arrowheads show the dumbbell-shaped mitochondria

used to investigate the association of mitochondrial aggregation and microtubule disassembly during RGV infection. Interestingly, when the colchicine was added, mitochondrial aggregation was blocked, and even mitochondrial distribution was also observed (Fig. 4B and C), whereas the viromatrix still existed in the RGV-infected cells. The data were further confirmed by ultrastructural observation (data not shown). It implies that mitochondrial aggregation in RGV-infected cells might be related to microtubules.

Induction of $\Delta\psi$m collapse in RGV-infected cells

In parallel with morphological changes, the difference of $\Delta\psi$m collapse was compared between the mock-infected and RGV-infected cells using flow-cytometry measurement with Rh123 staining. As shown in Fig. 5, the percentage of cells with $\Delta\psi$m collapse significantly increases from 12 h p.i., and along with the infection progress, the percentage gradually increases up to 30.13% until 24 h p.i. The results implicate that RGV infection induces $\Delta\psi$m collapse at the late stage of infection.

Activation of caspase-9 and caspase-3 during RGV-induced apoptosis

To analyze the roles of caspase during RGV-induced apoptosis, the activities of caspase-3 and caspase-9 were detected. As shown in Fig. 6, caspase-3 activity in the RGV-infected cells is early activated at 6 h p.i., and as the infection goes along, caspase-3 activity rises up to about five-fold in comparison to the mock-infected cells at 24 h p.i. Similarly, caspase-9 is also activated during RGV infection. However, only three-fold activity is heightened in comparison to the mock-infected cells at 12 h p.i., and then the activity level decreases till 24 h p.i.

NF-κB activation and intracellular Ca^{2+} increase during RGV-induced apoptosis

To determine whether NF-κB is activated to stimulate transcription following the RGV infection, we detected the luciferase activity using NF-κB-luc reporter gene. As shown in Fig. 7, the luciferase activity increases early at 6 h p.i. in the RGV-infected cells, and becomes the greatest at 18 h p.i. After that, the activity appears to decline at 24 h p.i. To normalize transfection efficiency, the expression level of β-Galactosidase was also detected, and no changes were found during the RGV infection (data not shown). The data indicate that RGV infection of FHM cells activates NF-κB dependent transcription.

Moreover, changes of intracellular free Ca^{2+} in the RGV-infected FHM cells were detected using Fluo-3AM. As shown in Fig. 8, in comparison with the mock-infected cells, the cytoplasmic Ca^{2+} rises gradually from 6 h p.i. to 24 h p.i. along with the infection progress.

Discussion

An increasing number of viruses are now known to induce apoptosis actively at the late stages of infection, and apoptosis is considered to play a critical role in pathogenesis of viral diseases [10]. In this study, the RGV-infected cells display characteristic morphological and

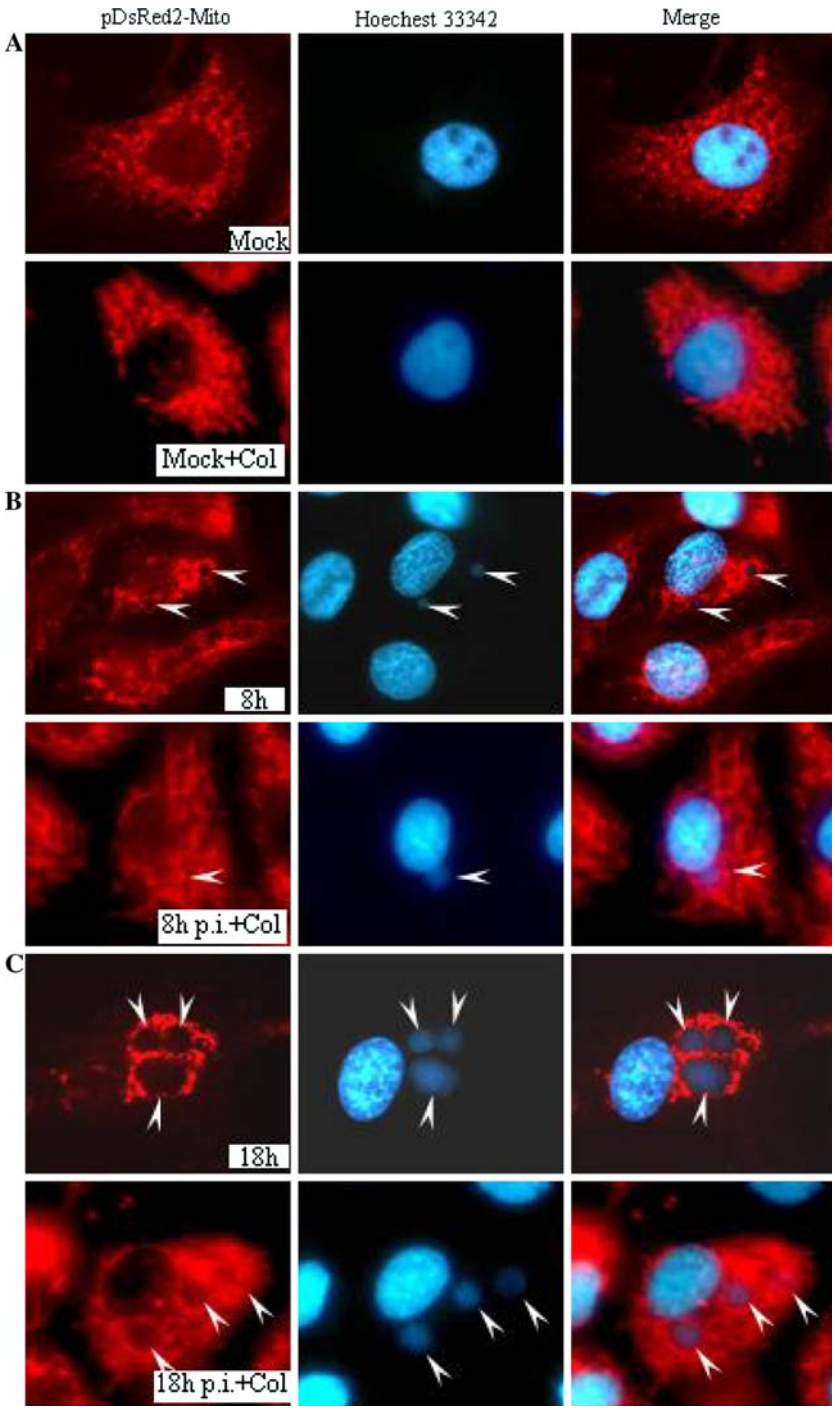

Fig. 4 Subcellular distribution of mitochondria of FHM cells in the absence or presence of colchicine (+Col). Left: mitochondrial fluorescence signals; middle: DNA staining pattern; right: images of the left and the middle were merged. Arrowheads indicate the nucleus and viromatrix

biochemical hallmarks of apoptosis, such as nuclear chromatin condensation, DNA fragmentation and formation of apoptotic bodies, suggesting that RGV-induced cell death should be mediated by apoptosis. Previously, some other members in family *Iridoviridae*, such as epizootic hematopoietic necrosis virus (EHNV), frog virus 3 (FV3), lymphocystis disease virus (LCDV) and red sea bream iridovirus (RSIV), were also proved to induce typical apoptosis during in vitro infection [14, 22–24].

Mitochondria are central to the physiology of eukaryotic organisms, and the fragmentation and internal ultrastructure changes have been observed in apoptotic cells [6, 25]. In the RGV-infected FHM cells, both of mitochondrial size and internal cristae number are reduced. Interestingly, significantly morphological changes of mitochondria also appear in the RGV-infected fish cells, and numerous dumbbell-shaped mitochondria are distributed around the viromatrix. Previous reports have indicated that changes of

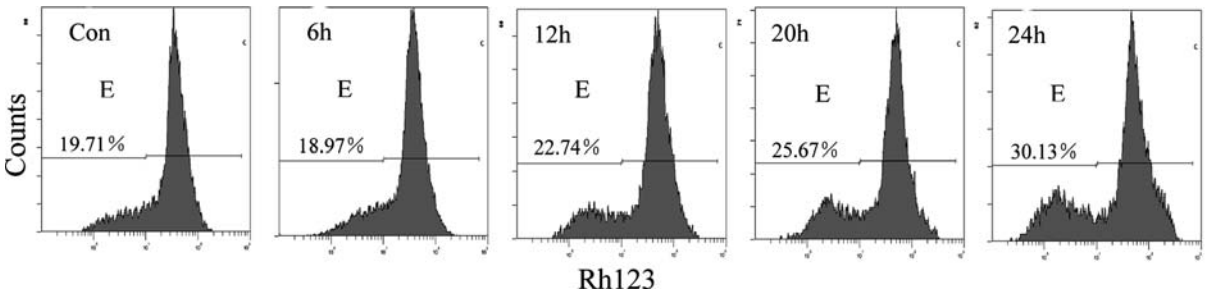

Fig. 5 Effect of RGV infection on $\Delta\psi$m in FHM cells. In each plot, the region of E shows the percentage of cells with decreased $\Delta\psi$m

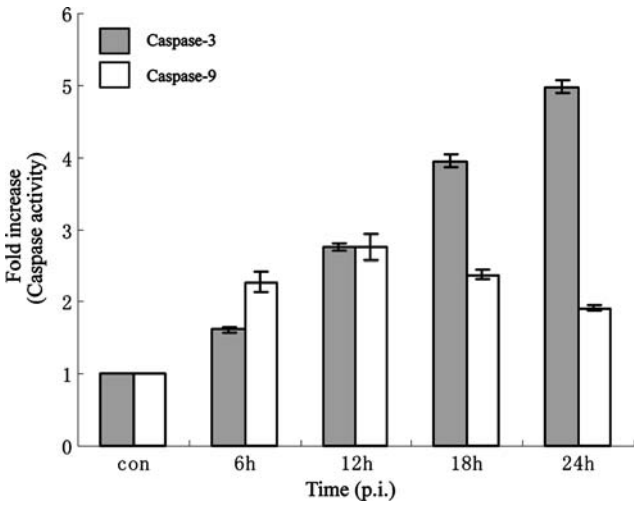

Fig. 6 Measurement of caspase-3 and caspase-9 activities in the RGV-infected FHM cells. Mock- and RGV-infected cells were collected at different times after infection and the levels of cleaved caspase substrate were measured. The data are expressed as fold increase compared to the corresponding values of caspase activity in mock-infected cells

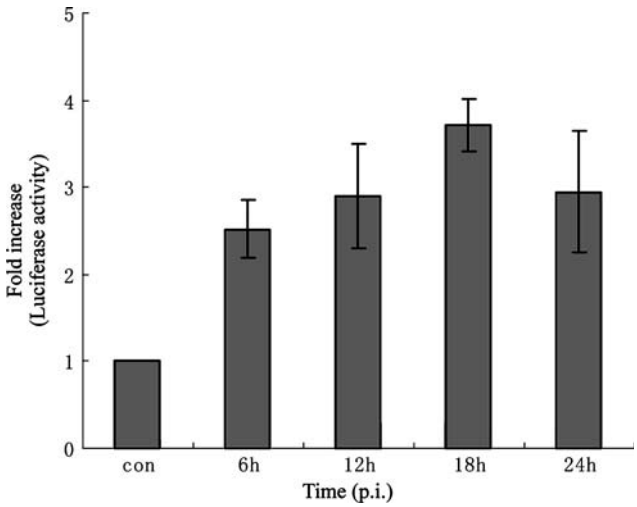

Fig. 7 Measurement of NF-κB activity in the RGV-infected FHM cells. Cells were lysed and the relative luciferase activity was detected. The data are expressed as fold increase compared to the corresponding values of luciferase activity in mock-infected cells

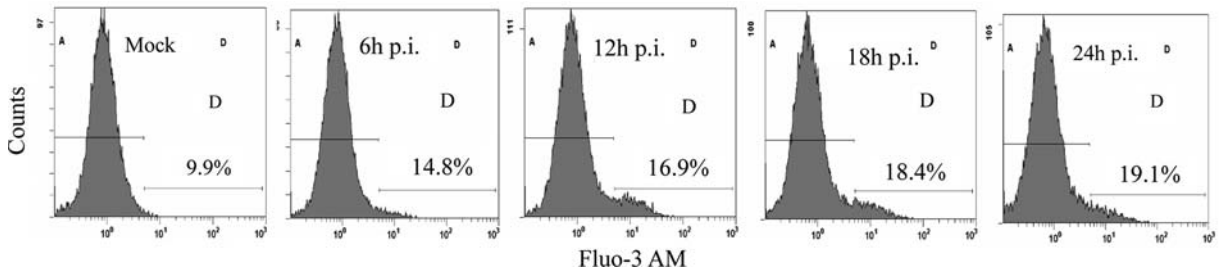

Fig. 8 Changes of intracellular Ca^{2+} in the RGV-infected FHM cells. In each plot, the region of D shows the percentage of cells with high Fluo-3 fluorescence intensity

the mitochondrial distribution not only provide the energy for virus pathogenesis, but also play important roles in the process of apoptosis [26, 27]. In the cases of the mammalian viruses, mitochondrial distribution changes and apoptosis occurrence have been observed during viral infection [28, 29]. In the RGV-infected cells, mitochondria are aggregated together, and associated with the viromatrix at the late stage of infection, and the aggregation can be blocked by colchicine. The data suggest that RGV infection might contribute to mitochondrial distribution change, and that the alteration might be mostly dependent on the microtubules.

Morphology and distribution changes of mitochondria are closely associated with their functions. Mitochondria have been suggested as the central control point of apoptosis [30]. Changes in $\Delta\psi$m are considered as an important event in the effect phase of apoptosis induced by many apoptotic stimuli, including virus infection [31]. Even if it is accompanied by $\Delta\psi$m increases at its early stage, apoptosis finally results in a $\Delta\psi$m collapse [32]. In the RGV-infected FHM cells, the $\Delta\psi$m collapse also appears similar changes. Previous reports showed that the $\Delta\psi$m collapse might shift the mitochondrial morphologic balance towards fragmentation [33]. Furthermore, caspase-9 and caspase-3 activities are heightened in the RGV-infected cells. Together, the data suggest that RGV infection should trigger mitochondrion-mediated apoptosis.

NF-κB transcription factors have been demonstrated to be major regulators of apoptosis [34–36], and intracellular Ca^{2+} homeostasis is also important for the control of apoptosis [37]. In the RGV-infected FHM cells, both NF-κB activation and intracellular Ca^{2+} increase were detected at different infection time. It implies that NF-κB activation and Ca^{2+} homeostasis disruption may play important roles in RGV-induced apoptosis.

In conclusion, the present study is the first report on mitochondrial fragmentation during virus-induced apoptosis in fish cells, and also reveals the detailed dynamics of the mitochondrion-mediated apoptosis triggered by an iridovirus in the family *Iridoviridae*.

Acknowledgments Grateful thanks for Ms. Zheng-Qiu Li and Xiu-Ping Yuan who provide great help. This study was supported by grants from the National Major Basic Research Program (2004CB117403), the National 863 High Technology Research Foundation of China (2006AA09Z445 and 2006AA100309), the National Natural Science Foundation of China (30671616 and U0631008) and the Project of Chinese Academy of Sciences (KSCX2-YW-N-021).

References

1. Hengartner MO (2000) The biochemistry of apoptosis. Nature 407:770–776
2. Youle RJ, Karbowski M (2005) Mitochondrial fission in apoptosis. Nat Rev Mol Cell Biol 6:657–663
3. Perfettini JL, Roumier T, Kroemer G (2005) Mitochondrial fusion and fission in the control of apoptosis. Trends Cell Biol 15:179–183
4. Alirol E, Martinou JC (2006) Mitochondria and cancer: is there a morphological connection? Oncogene 25:4706–4716
5. Karbowski M, Youle RJ (2003) Dynamics of mitochondrial morphology in healthy cells and during apoptosis. Cell Death Differ 10:870–880
6. Cereghetti GM, Scorrano L (2006) The many shapes of mitochondrial death. Oncogene 25:4717–4724
7. Delivani P, Adrain C, Taylor RC, Duriez PJ, Martin SJ (2006) Role for CED-9 and Egl-1 as regulators of mitochondrial fission and fusion dynamics. Mol Cell 21:761–773
8. Hay S, Kannourakis G (2002) A time to kill: viral manipulation of the cell death program. J Gen Virol 83:1547–1564
9. O'Brien V (1998) Viruses and apoptosis. J Gen Virol 79:1833–1845
10. Koyama AH, Fukumori T, Fujita M, Irie H, Adachi A (2000) Physiological significance of apoptosis in animal virus infection. Microbes Infect 2:1111–1117
11. Mi J, Li ZY, Ni S, Steinwaerder D, Lieber A (2001) Induced apoptosis supports spread of adenovirus vectors in tumors. Hum Gene Ther 12:1343–1352
12. Elankumaran S, Rockemann D, Samal SK (2006) Newcastle disease virus exerts oncolysis by both intrinsic and extrinsic caspase-dependent pathways of cell death. J Virol 80:7522–7534
13. Natoni A, Kass GEN, Carter MJ, Roberts LO (2006) The mitochondrial pathway of apoptosis is triggered during feline calicivirus infection. J Gen Virol 87:357–361
14. Chinchar VG, Bryan L, Wang J, Long S, Chinchar GD (2003) Induction of apoptosis in frog virus 3-infected cells. Virology 288:351–357
15. Du C, Zhang Q, Li C, Miao D, Gui J (2004) Induction of apoptosis in a carp leucocyte cell line infected with turbot (*Scophthalmus maximus* L.) rhabdovirus. Virus Res 101:119–126
16. Santi N, Sandtro A, Sindre H et al (2005) Infectious pancreatic necrosis virus induces apoptosis in vitro and in vivo independent of VP5 expression. Virology 342:13–25
17. Zhang QY, Xiao F, Li ZQ, Gui JF, Mao J, Chinchar VG (2001) Characterization of an iridovirus from the cultured pig frog *Rana grylio* with lethal syndrome. Dis Aquat Organ 48:27–36
18. Huang XH, Huang YH, Zhang QY (2006) Electron microscopic examination of the viromatrix of *Rana grylio* virus in a fish cell line. J Virol Methods 133:117–123
19. Zhang QY, Li ZQ, Jiang YL, Liang SC, Gui JF (1996) Preliminary studies on virus isolation and cell infection from disease frogs *Rana grylio*. Acta Hydrobiol Sin 20:390–392 (in Chinese with English abstract)
20. Du C, Zhang Q, Li C, Miao D, Gui J (2004) Induction of apoptosis in a carp leucocyte cell line infected with turbot (*Scophthalmus maximus* L.) rhabdovirus. Virus Res 101:119–126
21. Johnson LV, Wslsh ML, Bockus BJ, Chen LB (1981) Monitoring of relative mitochondrial membrane potential in living cells by fluorescence microscopy. J Cell Biol 88:526–535
22. Essbauer S, Ahne W (2002) The epizootic haematopoietic necrosis virus (Iridoviridae) induces apoptosis in vitro. J Vet Med B Infect Dis Vet Public Health 49:25–30
23. Hu GB, Cong RS, Fan TJ, Mei XG (2004) Induction of apoptosis in a flounder gill cell line by lymphocystis disease virus infection. J Fish Dis 27:657–662
24. Imajoh M, Sugiura H, Oshima S (2004) Morphological changes contribute to apoptotic cell death and are affected by caspase-3 and caspase-6 inhibitors during red sea bream iridovirus permissive replication. Virology 322:220–230
25. Martinou JC, Youle RJ (2006) Which came first, the cytochrome c release or the mitochondrial fission? Cell Death Differ 13:1291–1295
26. Murata T, Goshima F, Daikoku T, Inagaki-Ohara K, Takakuwa H, Nishiyamak Y (2000) Mitochondrial distribution and function in herpes simplex virus-infected cells. J Gen Virol 81:401–406
27. Haga N, Fujita N, Tsuruo T (2003) Mitochondrial aggregation precedes cytochrome c release from mitochondria during apoptosis. Oncogene 22:5579–5585
28. Rojo G, Chamorro M, Salas ML, Vinuela E, Cuezva JM, Salas J (1998) Migration of mitochondria to viral assembly sites in African swine fever virus-infected cells. J Virol 72:7583–7588
29. McCormick AL, Smith VL, Chow D, Mocarski ES (2003) Disruption of mitochondrial networks by the human cytomegalovirus UL37 gene product viral mitochondrion-localized inhibitor of apoptosis. J Virol 77:631–641

30. Desagher S, Martinou JC (2000) Mitochondrial as the central control point of apoptosis. Trends Cell Biol 10:369–377
31. Marchetti P, Hirsch T, Zamzami N et al (1996) Mitochondrial permeability transition triggers lymphocyte apoptosis. J Immunol 157:4830–4836
32. Skulachev VP (2006) Bioenergetic aspects of apoptosis, necrosis and mitoptosis. Apoptosis 11:473–485
33. Ishihara N, Jofuku A, Eura Y, Mihara K (2003) Regulation of mitochondrial morphology by membrane potential, and DRP1-dependent division and FZO1-dependent fusion reaction in mammalian cells. Biochem Biophys Res Commun 301:891–898
34. Dutta J, Fan Y, Gupta N, Fan G, Gelinas C (2006) Current insights into the regulation of programmed cell death by NF-kappaB. Oncogene 25:6800–6816
35. Karin M, Lin A (2002) NF-κB at the crossroads of life and death. Nat Immunol 3:221–227
36. Clarke P, Debiasi RL, Meintzer SM, Robinson BA, Tyler KL (2005) Inhibition of NF-kappa B activity and cFLIP expression contribute to viral-induced apoptosis. Apoptosis 10:513–524
37. Hail N Jr, Konopleva M, Sporn M, Lotan R, Andreeff M (2004) Evidence supporting a role for calcium in apoptosis induction by the synthetic triterpenoid 2-cyano-3,12-dioxooleana-1,9-dien-28-oic acid (CDDO). J Biol Chem 279:11179–11187